JOURNAL OF NANO- AND ELECTRONIC PHYSICS
Vol. **17** No 6, 06033(10pp) (2025)

ЖУРНАЛ НАНО- ТА ЕЛЕКТРОННОЇ ФІЗИКИ
Том **17** № 6, 06033(10cc) (2025)

OPEN ACCESS

REGULAR ARTICLE

Spectroscopic Characterization of Thermostimulated Transformation of Thin Films Based on Transition Metal Oxides Doped with Germanium

D.V. Khomenkov[1,*], D. Lehninger[2,3], L.Yu. Melnichuk[1], J. Heitmann[2], O.V. Melnichuk[1,†]

[1] *Mykola Gogol State University of Nizhyn, 16600 Nizhyn, Ukraine*
[2] *Institute of Applied Physics, TU Bergakademie Freiberg, 09599 Freiberg, Germany*
[3] *Fraunhofer Institute for Photonic Microsystems, 01109 Dresden, Germany*

(Received 12 September 2025; revised manuscript received 13 December 2025; published online 19 December 2025)

This work investigates the influence of germanium (Ge) doping on the structural properties of complex oxide films based on tantalum-zirconium oxide ($TaZrO_x$) with a comparative analysis including Ge-doped ZrO_2 films and their undoped counterparts. The thin films were deposited by magnetron sputtering and subjected to post-deposition annealing at 300-1000 °C in a nitrogen atmosphere. Fourier-transform infrared (FTIR) spectroscopy was employed to monitor changes in the vibrational modes associated with metal-oxygen bonding upon Ge incorporation. Shifts in the stretching modes, particularly within the 400-1000 cm^{-1} range, indicate site-selective incorporation of Ge into the Zr or Ta sublattices, modifying the local coordination and bonding environment. Comparative analysis suggests that Ge preferentially substitutes for Zr rather than Ta, consistent with thermodynamic trends in bond enthalpies and ionic radii. The results highlight the sensitivity of FTIR spectra to compositional variations in multi-cation oxide systems and provide insights into the structural role of Ge in modulating the vibrational and potentially functional properties of $TaZrO_x$-based films. These findings support the potential of Ge doping as a tunable parameter for tailoring the dielectric and optical properties of high-k complex oxides.

Keywords: High-k dielectrics, Ge doping, Magnetron sputtering, FTIR spectroscopy, Thin films, Post-deposition annealing.

DOI: 10.21272/jnep.17(6).06033 PACS numbers: 68.55. – a, 77.55. + f, 78.30. – j

1. INTRODUCTION

Transition metal oxides such as hafnium oxide (HfO_2) and zirconium oxide (ZrO_2), as well as their complex derivatives such as tantalum-zirconium oxides ($TaZrO_x$), attract considerable attention due to their potential applications in next-generation microelectronics, optoelectronic devices, and high-temperature dielectrics [1-11]. These materials combine high dielectric constants, wide band gaps, and thermal stability, making them suitable candidates for advanced electronic and optical applications.

Both HfO_2 and ZrO_2 are canonical high-k (k ~ 16-27) materials, exhibiting wide band gaps (~5.7-6.4 eV), thermal stability, and compatibility with silicon technology [1-3]. Although ZrO_2 and HfO_2 are chemically similar, their MO_2/Si (M = Zr, Hf) interface stabilities differ due to differences in their electronic structures [5]. Photoelectron spectroscopic experiments revealed the adiabatic electron affinity of HfO_2 to be 2.14 ± 0.03 eV and that of ZrO_2 to be 1.64 ± 0.03 eV. The excess electron in MO_2^- occupies an sd-type hybrid orbital localized on the M atom (M = Zr, Hf). At the same time, the structural parameters of ZrO_2 and HfO_2 and their vibrational frequencies are very similar. Upon excess-electron attachment, the M-O bond length increases by approximately 0.04 Å, the O-M-O angle increases by 2-4°, and the frequencies of all vibrational modes decrease, with stretching modes shifting by 30-50 cm^{-1} and the bending mode by 15-25 cm^{-1}. Therefore, while their electronic structures differ, the structural and vibrational characteristics of these oxides remain largely comparable.

Since HfO_2 is more ionic than ZrO_2, its crystallization can occur at lower temperatures. However, such behavior has been demonstrated experimentally only in a few studies [6]. This observation highlights the importance of comparing films grown under identical deposition conditions to draw reliable conclusions. A direct comparison is meaningful only when the films are prepared using the same technique, under similar deposition and post-deposition conditions.

For microelectronic applications, it is crucial to stabilize the amorphous structure of gate dielectrics to prevent high leakage currents. Since both oxides exhibit relatively low crystallization temperatures (300-350 °C), strategies to stabilize their amorphous structure are necessary [1,3]. Alternatively, maintaining the tetragonal phase, which provides a higher dielectric constant (k ~ 25), can also be advantageous, depending on the device requirements [7, 9].

The functional properties of HfO_2 and ZrO_2 can be further tailored through doping with isovalent ele-

* Correspondence e-mail: dmkhomen@gmail.com; khomenkov_dv@ndu.edu.ua
† mov310310@gmail.com

Cite this article as: D.V. Khomenkov et al., *J. Nano- Electron. Phys.* 17 No 6, 06033 (2025) https://doi.org/10.21272/jnep.17(6).06033

ments such as Si, Ge, and Sn [10-12]. Silicon doping at about 3-6 at. % preserves the amorphous HfO_2 structure during film growth at 300-500 °C and stabilizes it upon annealing at 800-900 °C [11, 12]. This stabilization arises from the formation of flexible Si-O covalent bonds, which inhibit HfO_2 crystallization by preventing the aggregation of Hf-O units.

Germanium doping of HfO_2 and ZrO_2 has shown particular promise in enhancing thermal stability and controlling crystallization behavior [6, 13]. The incorporation of germanium may delay the tetragonal-to-monoclinic phase transition upon cooling, modulate optical absorption edges, and alter vibrational features due to changes in the local coordination environment and bonding strength [10,14]. Moreover, doping with subvalent ions (Y^{3+}, Sc^{3+}, Ca^{2+}, Mg^{2+}) can also stabilize tetragonal and cubic phases at lower temperatures, although the accompanying formation of oxygen vacancies may introduce traps that impact device performance [17, 18]. Conversely, doping with supervalent ions such as Ta^{5+} or Nb^{5+} introduces electrons that can compensate existing oxygen vacancies, making these approaches attractive for fine-tuning material properties.

Several research groups have focused on developing Ge-doped high-*k* materials, primarily in the form of thin films or multilayer structures containing Ge nanocrystals embedded in an amorphous high-*k* host [13-17]. At high Ge contents, nanocrystal formation is observed and studied using transmission electron microscopy (TEM), X-ray diffraction (XRD), and Raman scattering [13, 16, 17]. Nevertheless, the host morphology and residual Ge content, which may significantly influence amorphous phase stability, are often less discussed.

Among the optical techniques used to investigate high-*k* materials, Fourier-transform infrared (FTIR) spectroscopy is particularly effective. For most films, FTIR spectra are recorded in transmission mode under normal incidence, with substrate contributions eliminated using instrument software. In certain studies, spectra recorded at the Brewster angle for Si-supported films allow overlapping LO and TO phonons to be resolved more clearly [18].

Recording FTIR spectra of Ge-doped high-*k* oxides under varying deposition or annealing conditions enables the monitoring of M-O (M = Hf, Zr, Ta) and Ge-O vibrational modes during film growth or post-deposition transformation. This approach also allows assessment of the effects of Ge content. For instance, Ref. [19] reports that increasing Ge in HfO_2 films leads to new absorption bands near 500-600 cm^{-1} associated with Ge-O stretching modes. Thermal annealing induces further changes in the spectra, such as peak sharpening or shifts, indicating improved crystallinity or phase separation [19]. Consequently, FTIR provides a sensitive fingerprint for detecting phase transitions and doping-induced disorder in high-*k* oxides.

The situation becomes more complex and scientifically rich in the case of ternary or quaternary oxides like $TaZrO_x$, where multiple cation sublattices may compete or cooperate under doping. The Ta-O and Zr-O bonds contribute to broad absorption bands typically centered between 400-800 cm^{-1}, and substitution of Zr^{4+} (ionic radius ≈0.72 Å) or Ta^{5+} (≈0.64 Å) by Ge^{4+} (ionic radius ~0.53 Å) can introduce substantial lattice distortion. Moreover, Ge doping may lead to the formation of substoichiometric oxides or secondary phases such as GeO_2 or Ge_xO_x clusters, which modify the FTIR spectra. These changes can manifest as additional peaks in the 700-900 cm^{-1} region, often attributed to Ge-O-M (M = Zr, Ta) stretching vibrations or interstitial-Ge related bonds.

Previous studies have indicated that germanium can exhibit amphoteric behavior, depending on its oxidation state and the annealing atmosphere. Under reducing conditions or during low-temperature growth, Ge may substitute into cation sites or promote oxygen vacancy formation. Conversely, oxidizing post-annealing favor(s) the formation of Ge^{4+} and GeO_2-like domains, which are readily detected by FTIR due to characteristic asymmetric stretching modes near 850-880 cm^{-1}.

In addition, Ge doping can influence defect formation energies and charge compensation mechanisms in $TaZrO_x$ systems. First-principles calculations suggest that germanium can alter the formation energy landscape of oxygen vacancies, potentially enhancing ionic conductivity or dielectric robustness. Such modifications are expected to manifest in FTIR spectra as broader absorption features or altered LO-TO (longitudinal-optical vs. transverse-optical) splitting in polar vibrational modes.

Beyond structural effects, Ge doping can also modify the dielectric and optical properties of complex oxides. Ellipsometry studies have shown that increasing Ge content can lead to a blue-shift in the absorption edge, which might indicate quantum confinement effects or defect passivation. Complementary FTIR data support this by revealing subtle changes in phonon dispersion and intensity across the infrared range.

Recent studies have begun to systematically explore these relationships. It demonstrated in HfO_2 thin films that controlled Ge incorporation leads to distinctive vibrational modes not present in undoped films, especially after thermal annealing [6]. Similarly, work on ZrO_2-Ta_2O_5 composites by other researchers has shown a progressive evolution of FTIR signatures with increasing Ge content, which correlates with changes in microstructure observed via transmission electron microscopy (TEM) and Raman spectroscopy.

Despite growing interest, relatively few studies have focused on the combined system of Ge-doped $TaZrO_x$. Yet, its investigation is both timely and important, given the complex phase behavior and potential functional applications of this ternary oxide. By integrating FTIR spectroscopy with complementary techniques such as XRD, Raman spectroscopy, and spectroscopic ellipsometry, we can gain comprehensive insight into how germanium affects local bonding, disorder, and vibrational coupling in these systems.

In this work, we present a detailed FTIR analysis of Ge-doped $TaZrO_x$ films grown by RF magnetron sputtering, focusing on how the spectral features evolve with varying Ge concentration and post-deposition annealing. By comparing these spectra with those of undoped reference materials ($TaZrO_x$ and ZrO_2), we aim to elucidate the role of Ge in reshaping the vibrational landscape and to establish structure-property correlations relevant to dielectric and optical applications.

2. EXPERIMENTAL DETAILS

Undoped and Ge-doped high-k oxide films were fabricated using a RF magnetron sputtering system, equipped with three plasma sources carrying 3″ Ge, high-k (ZrO_2 or ZrO_2-Ta_2O_5 mixed target) and SiO_2 targets, respectively. These targets were arranged confocally above the substrate in sputtering chamber. Film deposition was performed in "top-down" configuration in an argon plasma (with argon flow of 20 sccm), on rotated substrate without its heating, at a pressure of $5.2 \cdot 10^{-3}$ mbar. Prior to deposition, each 6″ ⟨100⟩ silicon wafer underwent to a standard RCA cleaning procedure, was dipped in diluted hydrofluoric acid, and immediately transferred to an oxidation chamber to grow a 3-nm SiO_2 layer by dry oxidation. The mixed ZrO_2-Ta_2O_5 target contains of 17 at. %. of Ta. The ZrO_2 target was framed with Si ring to minimise target charging during sputtering.

Undoped ZrO_2 and $TaZrO_x$, as well as SiO_2 layers were deposited by sputtering only the ZrO_2, ZrO_2-Ta_2O_5 or SiO_2 target, respectively. The power density for each oxide target was 3.3 W/cm². For Ge doping, the Ge target was sputtered with power density of 0.9 W/cm².

To prevent the evaporation of volatile GeO and the oxidation of Ge during annealing, all films were capped by a 10-nm SiO_2 layer.

All the films had thicknesses approximately 500 nm, achieved by fine tuning of deposition time (with second-level accuracy). Additional details on film growth can be found elsewhere [4, 13].

After film deposition, the wafer was cut into smaller pieces and annealed for 30 s in a rapid thermal processing system at temperatures between 500 to 1100 °C in a nitrogen atmosphere.

The film compositions were similar to those reported earlier from RBS analysis [4]. For $TaZrO_x$ films, the composition was 17 at. % Ta, 12 at. % Zr, and 71 at. % of O. For ZrO_2 films, it was 27 at. % Zr, 67 at. % O, and 6 % Si (originated from Si ring used as a frame for the ZrO_2 target). For Ge-doped ZrO_2, the composition was 15 at. % Ge, 17.5 at. % Zr, 62.9 at. % O, and 4 % Si, whereas for Ge-doped $TaZrO_x$ it was 10 at. % Ge, 14 at. % Ta, 10 at. % Zr, and 66 at. % O. The relative uncertainties in RBS experiments are about 5 % for the heavy elements (Ge, Zr, and Si), for which cross sections are well-known, and about 10 % for oxygen.

FTIR spectra were measured in the range of 460-4000 cm^{-1} using a Thermo Nicolet Nexus 750 (Thermo Fisher Scientific (formerly Thermo Electron Corporation), USA) and IRTracer-100 FTIR spectrometer (Shimadzu Company, Japan). The spectra were acquired in transmission mode at normal and Brewster incidence and were corrected on the signal from underlying Si substrate using built-in software of these spectrometers. Since all samples were grown in the same deposition unit, the comparison of obtained FTIR data is highly reliable.

3. RESULTS

3.1 Undoped ZrO_2 Films

Figure 1 shows the FTIR spectra of undoped ZrO_2 in initial state (as-deposited) and after RTA treatment at different temperatures. All the spectra exhibit a complex pattern.

The FTIR spectra of as-deposited ZrO_2 reveal two broad bands in the 460-750 cm^{-1} and 800-1250 cm^{-1} ranges, corresponding to Zr-O vibrations and Si-O (or possibly Si-O-Zr) vibrations, respectively (Fig. 1). These latter probably originate from Si incorporation during sputtering process due to target framing with Si ring. Besides, two weaker bands at approximately 1400 cm^{-1} and 1600 cm^{-1} as well as broad band in the 3600-4000 cm^{-1} were observed (not shown here), which can be attributed to Zr-OH vibrations arising from moisture incorporated in the film after deposition. Annealing leads to a gradual reduction of these bands and their disappearance after annealing at 600 °C.

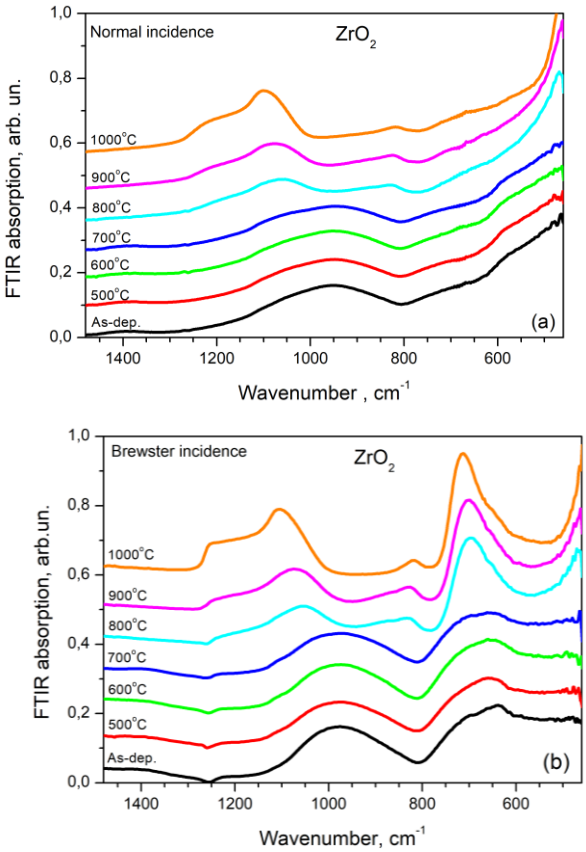

Fig. 1 – Evolution of FTIR spectra of ZrO_2 films with annealing temperature recorded under (a) normal and (b) Brewster incidence

Other FTIR bands remain largely unchanged within 500-700 °C temperature range. At 800 °C, the Zr-O-related band narrows, producing a distinct peak at ~450 cm^{-1} and a shoulder around 610-620 cm^{-1}. No peaks corresponding to the monoclinic ZrO_2 phase (760-780 cm^{-1}) are observed in any annealed samples. Based on the assignment of Zr-O vibrations (Table 2), these results indicate that the ZrO_2 host adopts either the tetragonal or cubic phase after annealing.

3.2 Undoped $TaZrO_x$ Films

Figure 2 demonstrates the FTIR spectra in the 460-1480 cm^{-1} range for undoped $TaZrO_x$ films, as-deposited and those annealed at temperatures from

500 °C to 1000 °C. It is seen that the spectrum for as-deposited film is broad and the main vibration bands appear in the 460-1000 cm^{-1} range. The spectrum is mostly featureless, indicating an amorphous structure. In contrast to ZrO_2 films, any OH-related features in the 1400-1600 cm^{-1} and 3600-4000 cm^{-1} ranges were not observed, which likely reflects a higher densification of the film. Furthermore, the contribution of Si-O vibrations is relatively weak being due to SiO_2 interfacial and cap layers only (Fig. 2). This corroborates with the RBS data mentioned above.

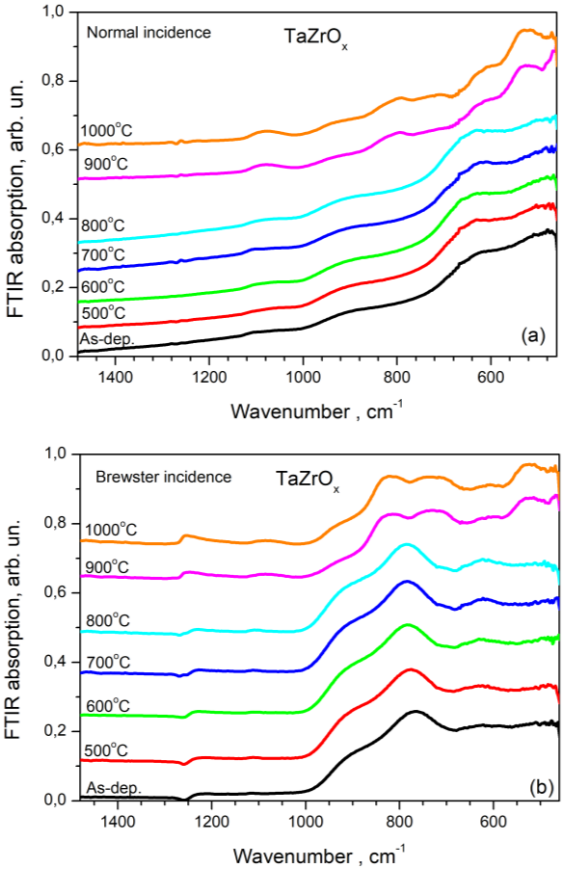

Fig. 2 – Evolution of FTIR spectra of $TaZrO_x$ films with annealing temperature recorded under (a) normal and (b) Brewster incidence

Annealing at 500-800 °C results in the slight increase in absorption intensity across the 400-1000 cm^{-1} region. Weak shoulders appear near ~ 630 cm^{-1} and ~ 880 cm^{-1}, which can be attributed to Ta-O vibrations in sub-oxides or mixed Ta-Zr bonding environments. No significant change in the high-wavenumber region (~ 1200-1600 cm^{-1} and 3600-4000 cm^{-1}), consistent with the absence of OH groups. When annealing temperature increases up to 900-1000 °C, vibration bands at ~ 630 cm^{-1} and ~ 880 cm^{-1} become more pronounced, suggesting increased contribution from Ta-O vibrational modes and possible structural reordering. Overall spectral shape remains broad, indicating the film remains largely amorphous. At the same time the contribution of Si-O vibration bands at 1080 and 1260 cm^{-1} increases that is the evidence of the reordering of Si-O bonds in interfacial and cap layers (Fig. 2a).

Analysis of the FTIR spectra recorded under Brewster incidence supports this behaviour (Fig. 2b). The shape of the FTIR spectra remains nearly unchanged up to 800 °C, while significant transformation occurs at 900 °C. The FTIR spectra for the films annealed at 900 °C and 1000 °C become to be similar also. Thus, with increasing annealing temperature, the films' structure changes in a step-like manner when annealing temperature exceeds 800 °C.

Although comprehensive information regarding FTIR band assignment in $TaZrO_x$ is limited, particularly for films with varying Ta:Zr ratios, the vibrational modes of pure ZrO_2 and Ta_2O_5 can be used as references (Table A1). A comparison of the FTIR spectra of ZrO_2 and $TaZrO_x$ films (Figs. 1 and 2) suggests that the bands centered at approximately 630-640 cm^{-1} and 880-900 cm^{-1} are most likely associated with Ta-O vibrations.

Since all samples are covered with similar 10 nm SiO_2 capping layers, the broad absorption in the 800-1000 cm^{-1} region is more reasonably attributed to Ta-O vibrations in sub-oxides such as TaO or TaO_2 rather than to Si-O vibrations. However, the possible formation of Si-O-Ta bonds near Si substrate and near SiO_2 cap layer cannot be ruled out. Considering the higher atomic mass of Ta compared with Zr, the vibrational frequency of Si-O-Ta is expected to be lower than that of Si-O-Zr.

Previous studies of the similar samples by XRD method [13] revealed that the crystallization behavior of $TaZrO_x$ strongly depends on the Zr/(Ta+Zr) ratio. For Zr/(Ta+Zr)=0.19, the film remains amorphous below 800 °C, while above 800 °C a hexagonal Ta_2O_5 phase appears. For Zr/(Ta+Zr) = 0.33, Ta_2O_5 crystallization begins at 900 °C. For Zr/(Ta+Zr) = 0.6, no crystalline Ta_2O_5 peaks are detected even after annealing at 900 °C, and instead the ZrO_2 phase adopts an orthorhombic structure, which already appears at 800 °C. Based on these reference data, our $TaZrO_x$ films are expected to exhibit consistently amorphous Ta_2O_5 components regardless of the Ta content, whereas the ZrO_2 component can crystallize in phases other than monoclinic. Thus, even with varying Ta/Zr ratios, the amorphous nature of Ta_2O_5 is preserved, while ZrO_2 may form cubic, tetragonal or orthorhombic polymorphs depending on annealing conditions.

3.3 Ge-doped ZrO_2 Films

Figure 3 shows the evolution of the FTIR spectra of Ge-doped ZrO_2 films with annealing. Similar to the undoped films, the significant changing appears at 700 °C. No OH-related bands were observed in Ge-doped ZrO_2 contrary to those in undoped counterparts that testifies to the higher film density.

For annealed Ge-doped ZrO_2 samples, the first significant spectral changes are detected at 700 °C when the Si-O related band near 1200 cm^{-1} increases in intensity (Fig.3). At 800 °C, additional bands in the 500-550 cm^{-1} and 800-1000 cm^{-1} range appear being peaked near 530, 820 and ~ 860-880 cm^{-1}. The latter feature was found in the samples with higher Ge content [6] being more pronounced with higher Ge concentration. No other distinct changes are detected at lower annealing temperatures.

At 900-1000 °C, the FTIR spectra change significantly. Strong vibration band near 720-740 cm^{-1} with a shoulder near 820 cm^{-1} is revealed. It is accompanied by the strong rise in intensity for Si-related bands in the 1000-1200 cm^{-1} range (Fig.3). Such transformation of the FTIR spectra shape can originate from the crystallization of ZrO_2 host despite of the presence of some Si content that usually stabilised its amorphous nature. It is evidently that the phase separation in SiO_2 and ZrO_2 phases occurs in these films similar to that reported in [20].

3.4 Ge-doped $TaZrO_x$ Films

The FTIR spectra of Ge-doped $TaZrO_x$ films (Fig. 4) show that Ge doping causes their featureless shape for as-deposited films. OH-related features are absent across all Ge-$TaZrO_x$ samples. Annealing at 500-700 °C did not affect the spectra shape (Fig. 4). But the step-like transformation occurs at 800 °C, whereas higher annealing temperatures did not change the shape of FTIR spectra.

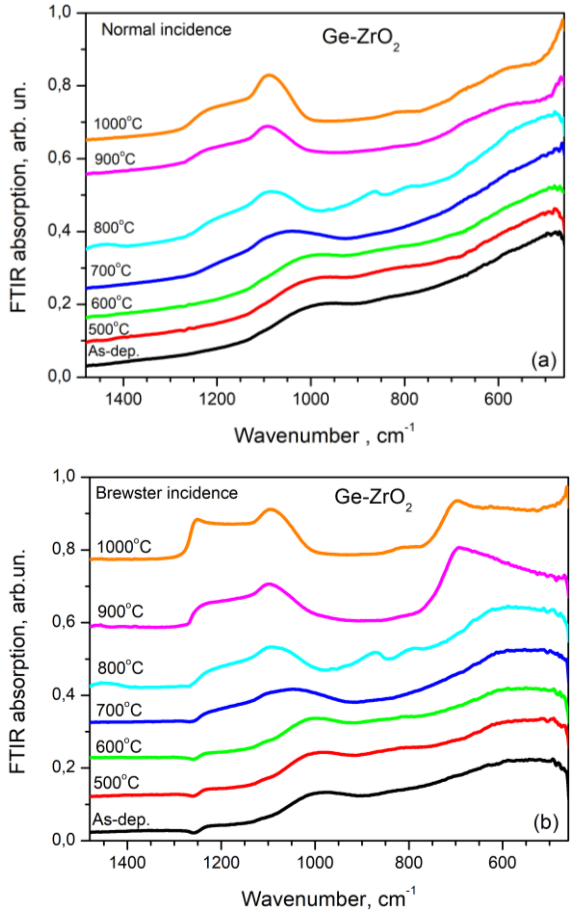

Fig. 3 – Evolution of FTIR spectra of Ge-doped ZrO_2 films with annealing temperature recorded under (a) normal and (b) Brewster incidence

Indeed, upon annealing at 800 °C, changes occur primarily in the low-wavenumber region. The band at ~640-660 cm^{-1} decreases in intensity for Ge-$TaZrO_x$ samples annealed at 800 °C, accompanied by a relative enhancement of features in the 500-600 cm^{-1} and 820-840 cm^{-1} range (Fig. 4a).

No distinct band in the 800-1000 cm^{-1} region is detected for Ge-doped $TaZrO_x$ films, in contrast to Ge-doped ZrO_2. At the same time, the contribution of Si-O bands increases due to reordering in the corresponding SiO_2 layers. The analysis of the FTIR spectra recorded under Brewster incidence showed that the transformation can originate form the rearrangement of the different vibration Zr-O, Ta-O, Ge-O and their mixed vibration bands.

3.5 Comparison of FTIR Spectra of Undoped and Doped Films

The comparison of the Ge-doped ZrO_2 and Ge-doped $TaZrO_x$ sets shows that Ge doping appears to prevent the appearance of OH-related vibration bands. This effect is likely due to the higher packing density of Ge-doped films compared with Ge-free films, particularly for pure ZrO_2. Doping with Ge leads to progressively more featureless FTIR spectra, which can be interpreted as evidence for enhanced stability of the amorphous phase in the host matrix.

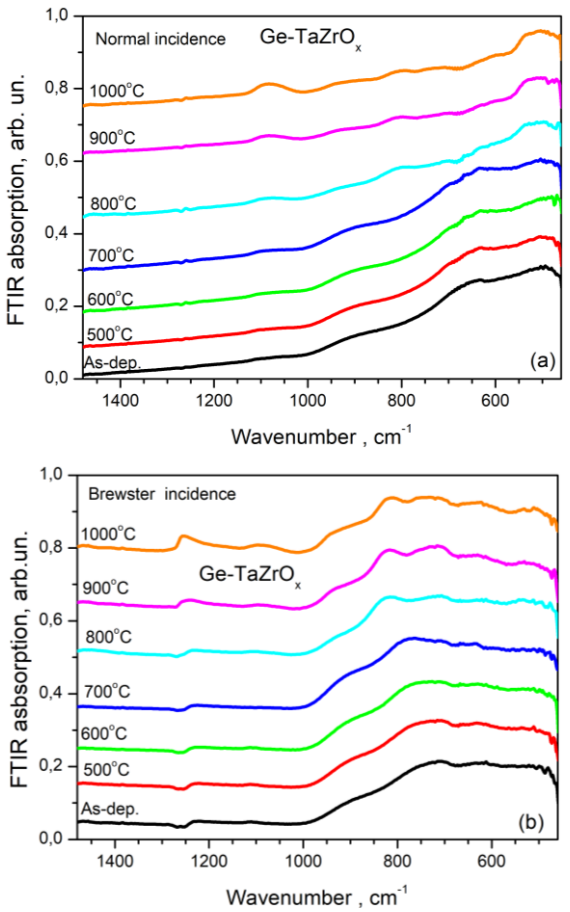

Fig. 4 – Evolution of FTIR spectra of Ge-doped $TaZrO_x$ films with annealing temperature recorded under (a) normal and (b) Brewster incidence

Significant transformations in the FTIR spectra occur starting from $T_a = 800$ °C. In Ge-ZrO_2 samples annealed at 800 °C, an additional band attributed to Ge-O vibrations of a glassy GeO_2 phase (Table A1).

Further comparison of Ge-ZrO_2 and Ge-$TaZrO_x$ films shows that the main distinction at 800 °C is the

emergence of a band in the 800-1000 cm^{-1} range (Fig. 3b-d), peaking at ~ 860-880 cm^{-1}. Its intensity increases with Ge content in Ge-ZrO_2 films and may correspond to Ge-O vibrations. In contrast, this band is absent in Ge-doped $TaZrO_x$ samples (Fig. 4), suggesting that in Ge-doped $TaZrO_x$ films either less Ge is incorporated into the host lattice that corroborate with RBS data. Thus, phase separation is less visible compared with Ge-doped ZrO_2.

Ge-doped $TaZrO_x$ films exhibit higher stability under annealing (Fig.4). This corroborates with the result of Ref. [6] where the films with higher Ge content demonstrated similar shape of FTIR spectra whatever annealing temperature. However, there is a redistribution of Ta-O and Ge-O vibrations appeared as a decrease in intensity of the ~630 cm^{-1} band in Ge-doped $TaZrO_x$ samples annealed at 800 °C. This may result from redistribution of Ta-O vibration intensity and an increase in the contribution of the ~ 550 cm^{-1} component. However, in 500-600 cm^{-1} spectral range, Ge-O and Ta-O bands overlap with those related to Zr-O vibrations (Fig. 5, Table 1).

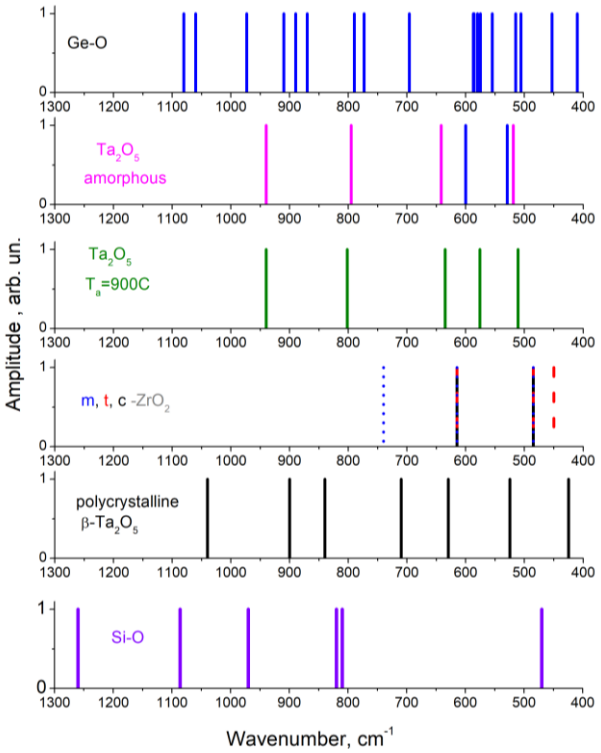

Fig. 5 – Schematic presentation of different vibrations related to oxides of Zr, Ta, Ge and Si. Assignments of the bands is given in Table 1

4. DISCUSSION

4.1 Vibrational Considerations and Bond-Mass Effects

The vibrational behavior of metal-oxygen networks follows classical mass-spring principles, whereby the frequencies of M-O-M stretching modes depend on the reduced mass of the vibrating pair. Accordingly, the substitution of heavier cations such as Zr or Ta by lighter Ge atoms ($m_{Ge} < m_{Zr} < m_{Ta}$) leads to higher characteristic vibrational frequencies. This manifests in the expected blue-shift of Zr-O-Ge or Ta-O-Ge modes relative to the Zr-O-Zr or Ta-O-Ta vibrations found in the corresponding undoped oxides. Well-established spectral features of Ge-O bonds include the well-known triplet of hexagonal GeO_2 at 515, 555, and 587 cm^{-1}, the broader merged band typical for amorphous GeO_2, and additional bands in the 860-1080 cm^{-1} region for crystalline Ge-based oxides (Table 1). These serve as benchmarks for interpreting the more complex vibrational responses in Ge-doped ZrO_2 and $TaZrO_x$ films, where the local bonding environment is strongly affected by both composition and structural disorder. Besides, we can compare spectra with undoped and Ge-doped HfO_2 since in terms of vibrational properties HfO_2 and ZrO_2 are similar [5].

4.2 Undoped ZrO_2 and $TaZrO_x$ Films

The vibrational characteristics of the undoped ZrO_2 and Ta-Zr mixed oxides establish a crucial reference point for understanding compositional and structural changes introduced by Ge doping. A notable distinction between the two systems is the absence of hydroxyl-related bands in $TaZrO_x$ films. Whereas ZrO_2 exhibits OH absorption features near 1400-1600 cm^{-1} and 3600-4000 cm^{-1}, the Ta-containing films lack such signatures, indicating intrinsically higher packing density and reduced porosity. This behavior aligns with the known densification tendency of Ta_2O_5 and its suboxides [30].

Additional FTIR features near 640-660 cm^{-1} and 880-900 cm^{-1} reflect the presence of Ta-O bonds in Ta_2O_5-like units or TaO_x species. The broad absorption spanning 800-1000 cm^{-1} is dominated by TaO_x modes rather than Si-O vibrations, as all samples contain identical SiO_2 capping and only Ta-containing films exhibit this response. In the mixed $TaZrO_x$ network, Zr-O-Ta vibrations are expected to occur at lower frequencies than Zr-O-Zr modes due to the significantly larger mass of Ta. Nevertheless, such shifts may be partially obscured by limited Ta solubility in ZrO_2 or incomplete formation of a uniform solid solution.

The thermal stability of the amorphous state also differs markedly between the two oxides. Prior literature shows that Zr incorporation raises the crystallization temperature of Ta_2O_5, while Ta addition suppresses crystallization in ZrO_2. This mutual stabilization is fully consistent with the present results, where $TaZrO_x$ films remain amorphous over a temperature range at which pure ZrO_2 or Ta_2O_5 typically crystallize. These observations create a well-defined baseline for evaluating the additional effects of Ge incorporation.

4.3 Influence of Ge Doping on Vibrational Modes

The introduction of Ge into both ZrO_2 and $TaZrO_x$ films produces systematic modifications in their vibrational spectra. As predicted from mass-spring considerations, the partial substitution of Zr^{4+} or Ta^{5+} with lighter Ge^{4+} and smaller ionic radius (≈ 0.53 Å) relative to Zr^{4+} (≈ 0.72 Å) and Ta^{5+} (≈ 0.64 Å) leads to observable blue-shifts in the M-O-Ge vibrational modes, confirm-

ing that Ge actively participates in the metal-oxygen network and occupies multiple cationic environments. In Ge--doped ZrO_2 films annealed at 800 °C, broad bands near 500-550 cm^{-1} and 860-880 cm^{-1} appear, closely matching the characteristic signatures of Ge-O stretching in amorphous GeO_2 or Ge-rich units.

By contrast, Ge-doped $TaZrO_x$ films do not exhibit analogous Ge-O spectral features, even after high-temperature annealing. This absence indicates either stronger incorporation of Ge within the Ta-Zr-O matrix or suppression of GeO_2 segregation. Both scenarios imply significantly enhanced Ge solubility in the mixed oxide environment compared with pure ZrO_2. These results show that Ge modulates the local and medium-range structure in ways that depend sensitively on the chemical and structural state of the host oxide.

4.4 Amorphous Phase Stability and Spectral Broadening

A notable effect of Ge doping is the progressive broadening and featureless nature of the FTIR spectra, which correlates with enhanced amorphous-phase retention. Ge doping sharply enhances the stability of the amorphous phase in both oxide systems. For ZrO_2, increasing spectral sharpening after annealing at 800 °C typically signals the initiation of crystallization, with phonon features associated with tetragonal or monoclinic phases gradually emerging. However, in Ge-doped ZrO_2 films, phonon bands retain their broad, diffuse character even after high-temperature treatment, demonstrating that crystallization is effectively delayed or partially suppressed.

In Ge-doped $TaZrO_x$ films, the stabilizing effect of Ge is even more pronounced. Across the full annealing range explored, these films show negligible changes in peak positions, widths, or spectral shapes. Two complementary mechanisms explain this robust stabilization: (i) the incorporation of smaller Ge^{4+} ions introduce local lattice distortions that suppress the nucleation of ordered phases, and (ii) the inherent configurational complexity of the Ta-Zr cation mixture creates a rugged potential-energy landscape unfavorable for long-range structural ordering. Together, these factors lead to strong retention of the amorphous state, which is particularly important for designing stable high-k dielectric layers.

4.5 Interaction Between Cation-Oxygen Bonds

The FTIR spectra of the Ge-doped samples reflect a complex superposition of Zr-O, Ta-O, and Ge-O vibrational contributions. Redistribution of intensity in the 550-630 cm^{-1} region arises from the overlap and competition between these modes. Specifically, Zr-O-Ta linkages tend to shift spectral weight toward lower frequencies, while Ge incorporation introduces additional components at higher wavenumbers. The resulting envelopes are highly convolutional, especially in Ta-rich films, where broad TaO_x modes overlap with Ge-induced features (Table 1). This spectral complexity is fully consistent with an amorphous, multi-cation network lacking well-defined long-range order. The recording of the FTIR spectra under Brewster geometry reveals this tendency clearer. Besides, the previous study of similar films using Raman spectroscopy and XRD method confirmed the amorphous nature of the films annealed at temperatures below 800 °C [13].

4.6 Phase Evolution and Crystallization Behavior

Annealing treatments demonstrate distinct differences in phase evolution between Ge-doped ZrO_2 and Ge-doped $TaZrO_x$ samples. In the former ones, phonon features associated with monoclinic ZrO_2 begin to appear above 800 °C (Fig.3). Indeed, annealing at 900 °C and 1000 °C results in the appearance of phonon mode near 740-760 cm^{-1} specific for monoclinic phase only. Thus, a partial ordering occurs for the previously amorphous matrix. Notably, the monoclinic phase, normally the thermodynamically stable structure, is suppressed in the films annealed at lower temperatures. Apart of this, in ZrO_2 films the presence of some amount of Si was registered. Thus, even the Ge content is higher, additional Si effect on the amorphous phase stabilization cannot be ruled out. However, annealing of the ZrO_2-based films at 900 °C and 1000 °C showed that neither Ge nor Si can stabilize amorphous or tetragonal/cubic structure of ZrO_2. This can be due to complete phase separation in Ge- and Si-doped ZrO_2 films followed by the formation of SiO_2 and ZrO_2 phases and probably GeO_2 one, or even the evaporation of Ge due to formation of volatile GeO phase. Similar effect was found for the Ge-doped HfO_2 films prepared in the same deposition unit and studied by us recently [7], where additional investigation with Raman scattering methods revealed the significant decrease of the amplitude of Ge-related signal. Thus, one can assume the annealing of Ge-doped ZrO_2 at 900-1000 °C caused the Ge content decrease in these films, followed by the monoclinic ZrO_2 formation. To support this assumption, an additional study of the structure and chemical composition of such films is in progress.

In contrast, Ge-$TaZrO_x$ films remain largely amorphous even after annealing at temperatures below 800 °C, reflecting the inherently elevated crystallization temperature of the Ta-Zr oxide mixture. The presence of Ge further strengthens this resistance to ordering, indicating a synergistic effect between Ta and Ge in suppressing crystallization and phase separation. This exceptional amorphous stability has favorable implications for applications requiring uniform dielectric response and minimal grain-boundary formation.

At the same time, annealing at 900 and 1000 °C favors the appearance of well-defined vibration bands that are the features of the crystalline Ta- and Zr-related phase. However, ZrO_2 phase has the structure different than monoclinic one because no sharp peak at 740-760 cm^{-1} appeared. One can assume that this phase can be of higher symmetry (cubic or tetragonal, or even orthorhombic one). One cannot compare directly our results with those of Refs. [4, 13] for Ge-doped $TaZrO_x$ films, since in those works the films with higher Ge content were studied, however, one can address the tendency of the evolution of their host oxide and formation of T_2O_5 and ZrO_2 nanocrystalline phases after annealing at 800-900 °C that can support our assumptions. To support it, additional study of our films with XRD and/or TEM method is planned.

CONCLUSIONS

This work demonstrates how Ge incorporation fundamentally alters the structural evolution of ZrO_2 and $TaZrO_x$ thin films, with clear evidence of dopant-induced modifications in vibrational dynamics and phase stability. FTIR analysis confirms that Ge actively participates in the metal-oxygen framework, producing blue-shifted stretching modes consistent with the reduced cation mass of Ge relative to Zr and Ta. The emergence of Ge-related bands near 500-550 cm^{-1} and 860-880 cm^{-1} in Ge-ZrO_2 annealed at 800 °C reflects partial formation of Ge-O linkages and Ge-rich units, whereas their absence in Ge-$TaZrO_x$ indicates higher Ge solubility and stronger incorporation within the mixed-oxide network.

Ge doping markedly influences amorphous retention. While undoped ZrO_2 tends to crystallize upon high-temperature treatment, Ge-doped ZrO_2 films retain broad, featureless vibrational envelopes even after annealing, demonstrating delayed phase ordering. The effect is even more pronounced in Ge-$TaZrO_x$, where the amorphous state persists across the entire investigated temperature range, attributable to both local distortions introduced by Ge and the configurational complexity of the Ta-Zr cation mixture. Only at 900-1000 °C, do crystalline vibrational signatures appear, and in contrast to Ge-doped ZrO_2, the formed ZrO_2-related phase does not exhibit the characteristic monoclinic phonon at 740-760 cm^{-1}, suggesting the stabilization of a higher-symmetry polymorph or mixed-phase configuration.

Comparative behavior of the Ge-doped ZrO_2 and Ge-doped $TaZrO_x$ samples highlights that Ge is less stable in ZrO_2 under extreme annealing, likely undergoing segregation or volatilization (GeO formation), eventually allowing monoclinic ZrO_2 to be formed. This is also observed for the Ge0doped ZrO_2 films additionally doped with silicon.

In Ge-doped $TaZrO_x$ films, no analogous phase separation is observed, confirming that Ge acts as a structural stabilizer when Ta is present. This difference demonstrates that Ta-containing films are more robust hosts for Ge-mediated amorphous retention.

These findings establish Ge doping as a viable strategy for controlling structural disorder, delaying crystallization, and engineering vibrational behavior in high-k oxide thin films. The exceptional amorphous stability of Ge-doped $TaZrO_x$ in particular makes it an attractive platform for dielectric and optical applications where grain-boundary formation must be minimized. Planned XRD, Raman and TEM analysis will further clarify the high-temperature phase transformations and the eventual coordination environment of Ge in these complex oxide matrices.

APPENDIX A

Table 1 – Assignment of different FTIR vibration bands

Bond configuration	Spectral position, cm^{-1} (Vibration type)	Reference
Zr-O related bond vibration		
Zr-O monoclinic	350, 425, 520, 595, 740 (as-deposited) (20 °C) 335, 410, 505, 575, 740 (shoulder) (673 °C) 325, 400, 505, 575, 750 (910 °C)	[21]
Zr-O tetragonal	485, 615	
Zr-O cubic	450, 485, 615	
Si-O related bond vibration		
Si-O-Si	470 (rocking) (TO_1)	[22]
	820 (bending) (TO_2)	
	1086 (asymmetric) (TO_3)	
$Si-O^{1-}$	970 (terminal Si-O groups produced by network disruption)	[23]
Ta-O related bond vibration		
Ta-O	266, 500, 609, 672, 868 (amorphous Ta_2O_5)	[24]
	91, 214, 324, 530, 842 (nanocryst. Ta_2O_5)	
Ta-O-Ta, O≡3Ta	280 (amorphous), 210 (cryst)	[25]
O≡3Ta	640 (amorphous), 510 (cryst)	
Ta-O-Ta	790-1000 (amorphous); 810 (cryst)	
Ta=O	2340 (amorphous); 2335 (cryst)	
Ta-O (in β-Ta_2O_5 polycryst, 500 nm, on Si substrate), absorption	220; 325 shoulder; 380 weak; 425 shoulder; 525 strong; 630 shoulder; 710 shoulder; 840; 900 shoulder; 1040 shoulder	[26]
Ta-O	639-648 (TO_a phonon) in Ta_2O_5 amorphous film 778-794 (LO_a phonon)	[27]
Ta-O	519, 642 - amorphous Ta_2O_5 (TO phonons) 795, 940 - amorphous Ta_2O_5 (LO phonons) 511, 576, 635, 802, 940 - the same film annealed at 900°C	[28]
Ta-O-Ta, Ta-O	518, 640 and 870	[29, 30]
Ge-O related bond vibration		
Ge-O	515, 555 and 587 (triplet of hexagonal GeO_2) (stretching)	[25, 31]

Ge-O-Ge	580 (bending)	[19]
	870 (stretching)	
Ge-OH⁻ in $H_2GeO_4^{2-}$	1060-1080	[32]
Ge-O⁻	1060-1080 (non-bridging)	[33]
Ge-O	696 stretching (in $ZrGeO_4$)	[34]
Ge-O-Ge	575 bending (in $ZrGeO_4$)	
O-Ge-O	453 bending (in $ZrGeO_4$)	
Ge-O	410 (ν(M-O) in [MO_6])	[35]
	453 (δ(Ge-O) in [GeO_4])	
	506 (ν(Ge-O) in [GeO_4] glassy GeO_2)	
	502-580 shoulder (ν(Ge-O) in glassy GeO_2)	
	575 (ν(Ge-O) in [GeO_6])	
	586 (δ(Ge-O) in [GeO_4])	
	696 (ν(Ge-O) in $[GeO_4]^{3-}$ in orthogermanates)	
	doublet 773, 793 (ν(Ge-O) in metagermanates $[GeO_3]^{2-}$)	
	shoulder 790-890 (ν(Ge-O) in polygermanates)	
	910 (ν(Ge-O) in [GeO_4])	
	1060 (ν(Ge-O) in orthogermanates $[GeO4]^{2-}$)	
	1080 (ν(Ge-O) in orthogermanates $[GeO4]^{3-}$)	

REFERENCES

1. J. Robertson, *J. Vac. Sci. Technol. B* **18**, 1785 (2000).
2. D. Panda, T.-Y. Tseng, *Thin Solid Films* **531**, 1 (2013).
3. X. Zhao, D. Vanderbilt, *Phys. Rev. B* **65**, 075105 (2002).
4. D. Lehninger, D. Rafaja, J. Wünsche, F. Schneider, J. von Borany, J. Heitmann, *Appl. Phys. Lett.* **110**, 262903 (2017).
5. W. Zheng, K.H. Bowen, J. Li, I. Dąbkowska, M. Gutowski, *J. Phys. Chem. A* **109**, 11521 (2005).
6. L. Khomenkova, D. Lehninger, E. Agocs, P. Petrik, X. Portier, N. Korsunska, O. Melnichuk, F. Gourbilleau, J. Heitmann, *ECS Trans.* **97**, 49 (2020).
7. D. Khomenkov, L. Melnichuk, F. Gourbilleau, O. Melnichuk O. *MRS Adv.,* in press (manuscript ID: MRSA-D-25-00824) (2025).
8. J.L. Musfeldt, S. Singh, K.A. Smith, X. Xu, S.-W. Cheong, Z. Liu, D. Vanderbilt, K.M. Rabe, *Chem. Mater.* **37**, 1820 (2025).
9. D. Tsoutsou, G. Apostolopoulos, S. Galata, P. Tsipas, A. Sotiropoulos, G. Mavrou, Y. Panayiotatos, A. Dimoulas, *Microelectron. Eng.* **86**, 1626 (2009).
10. P. Li, I.-W. Chen, J.E. Penner-Hahn, *J. Am. Ceram. Soc.* **77**, 1281 (1994).
11. L. Khomenkova, P. Normand, F. Gourbilleau, A. Slaoui, C. Bonafos, *Thin Solid Films* **617**, 143 (2016).
12. D. Khomenkov, L. Melnichuk, L. Khomenkova, F. Gourbilleau, O. Melnichuk, *Semicond. Phys. Quantum Electron. Optoelectron.* **28**, 402 (2025).
13. D. Lehninger, F. Honeit, D. Rafaja, V. Klemm, C. Röder, L. Khomenkova, F. Schneider, J. von Borany, J. Heitmann, *MRS Bull.* **47**, 773 (2022).
14. J.M. Purswani, A.P. Pons, J.T. Glass, R.D. Evans, and J.D. Cogdell, *MRS Proc.* **811**, D3.8 (2004).
15. L. Khomenkova, D. Lehninger, O. Kondratenko, S. Ponomaryov, O. Gudymenko, Z. Tsybrii, V. Yukhymchuk, V. Kladko, J. von Borany, J. Heitmann, *Nanoscale Res. Lett.* **12**, 196 (2017).
16. C. Palade, A.-M. Lepadatu, A. Slav, V.S. Teodorescu, T. Stoica, M.L. Ciurea, D. Ursutiu, C. Samoila, *Materials* **14**, 7040 (2021).
17. W.K. Chim, *Nanoscale* **17**, 4195 (2025).
18. L. Khomenkova, N. Korsunska, C. Labbé, X. Portier, F. Gourbilleau, *Appl. Surface Sci.* **471**, 521 (2019).
19. S. Miyazaki, K. Sakamoto, K. Shiba, and M. Hirose, *Thin Solid Films* **255**, 99 (1995).
20. F. Del Monte, W. Larsen, J.D. Mackenzie, *J. Am. Ceram. Soc.* **83**, 1506 (2000).
21. D.W. Liu, C.H. Perry, R.P. Ingel, *J. Appl. Phys.* **64**, 1413 (1988).
22. P.G. Pai, S.S. Chao, Y. Takagi, G. Lucovsky, *J. Vac. Sci. Technol. A* **4**, 486 (1986).
23. G. Lucovsky et al., *Surface Sci.* **566-568**, 772 (2004).
24. T.J. Bright, J.I. Watjen, Z.M. Zhang, C. Muratore, A.A. Voevodin, D.I. Koukis, D.B. Tanner, D.J. Arenas, *J. Appl. Phys.* **114**, 083515 (2013).
25. H. Ono, K.I. Koyanagi, *Appl. Phys. Lett.* **77**, 1431 (2000).
26. W. H. Knausenberger and R. N. Tauber, *J. Electrochem. Soc.* **120**, 927 (1973).
27. E. Franke, C.L. Trimble, M.J. DeVries, J.A. Woollam, M. Schubert, F. Frost, *J. Appl. Phys.* **88**, 5166 (2000).
28. R.A.B. Devine, *Appl. Phys. Lett.* **68**, 1924 (1996).
29. A. Cheikh, J. Gonçalves, C. Labbé, X. Portier, P. Marie, C. Frilay, O. Debieu, S. Duprey, W. Jadwisienczak, D. Ingram, J. Cardin, *J. Alloy. Compd.* **1040**, 183273 (2025).
30. H. Szymanowski, O. Zabeida, J.E. Klemberg-Sapieha, L. Martinu, *J. Vac. Sci. Technol. A* **23**, 241 (2005).
31. S.P. Mukherjee, A.S. Glass, M.D. Low, *J. Am. Ceram. Soc.* **73**, 242 (1990).
32. O.H. Johnson, *Chem. Rev.* **51**, 431 (1952).
33. K.E. Lipinska-Kalita, *J. Non-Cryst. Solids* **119**, 41 (1990).
34. R. Hubin, P. Tarte, *Spectrochim. Acta A* **27**, 683 (1971).
35. E.V. Frolova, V.S. Gurin, L.S. Ivashkevich, V.V. Sviridov, *Proc. SPIE* **4804**, 81 (2002).

Спектральні особливості термостимульованого фазового перетворення тонких плівок на основі оксидів перехідних металів, легованих германієм

Д.В. Хоменков[1], Д. Ленінгер[2,3], Л.Ю. Мельничук[1], Й. Хайтманн[2], О.В. Мельничук[1]

[1] *Ніжинський державний університет імені Миколи Гоголя, 16600 Ніжин, Україна*
[2] *Інститут прикладної фізики Технічного університету Гірничої академії Фрайберга, 09599 Фрайберг, Німеччина*
[3] *Фраунгофер Інститут фотонних мікросистем, 01109 Дрезден, Німеччина*

У роботі методом інфрачервоної спектроскопії з перетворенням Фур'є (FTIR) досліджено вплив легування германієм та термічних обробок на структурні властивості багатокомпонентних плівок на основі ZrO_2 та $TaZrO_x$, одержаних методом магнетронного напилення. Термічні обробки було проведено в атмосфері азоту за температур 300-1000 °C. Встановлено, що зсуви смуг коливань у діапазоні 400-1000 $см^{-1}$ свідчать про вбудовування атомів Ge у підґратки Zr або Ta, що призводить до зміни у локальному оточенні та характеру хімічних зв'язків. Порівняльний аналіз спектрів інфрачервоного поглинання нелегованих та легованих германієм зразків показує, що у $TaZrO_x$ матриці германій переважно заміщує цирконій, а не тантал, що узгоджується з термодинамічними параметрами цих оксидних матеріалів. Отримані результати демонструють високу чутливість спектрів інфрачервоного поглинання до змін в їх хімічному складі. Це дозволяє встановити особливості структурної трансформації плівок на основі ZrO_2 та $TaZrO_x$ при їх легуванні германієм та передбачити його вплив на функціональні характеристики цих діелектриків. Зроблено висновок, який вказує на перспективність легування германієм матеріалів із високою діелектричною сталою для цілеспрямованої зміни їх діелектричних та оптичних властивостей.

Ключові слова: Діелектрики з високою діелектричною сталою, Легування германієм, Магнетронне напилення, Інфрачервона спектроскопія з перетворенням Фур'є, Тонкі плівки, Термічні відпали.